Mineralogia, vol. 53, 2022, 20-35 *Original Paper*

DOI: 10.2478/mipo-2022-0003

Mineralogical and geochemical evidence for two-stage silicification of serpentinized peridotites from the Szklary Massif (NE Bohemian Massif)

Błażej Cieślik[1*]

Jakub Kierczak[1]

Anna Pietranik[1]

[1]University of Wrocław, Institute of Geological Sciences, pl. Maksa Borna 9, 50-204 Wrocław, Poland
*Corresponding author: blazej.cieslik2@uwr.edu.pl

Abstract

Previously unknown exposures of silicified serpentinites have been documented within the Szklary Massif, which is a fragment of the tectonically dismembered Central Sudetic Ophiolite (NE Bohemian Massif). On the basis of textural, mineralogical and chemical differences, two types of silicified serpentinites have been distinguished in this study (Type I and Type II). Type I is characterized by well-preserved primary minerals cut by numerous veinlets filled with microscale euhedral quartz crystals. Studied samples of Type I are enriched in silica (from 62 to 69 wt.% SiO_2) and depleted in magnesium (from 10 to 19 wt.% MgO) in comparison to serpentinized peridotites from the Szklary Massif. Type II is almost exclusively composed of amorphous or poorly crystalline silica, with microquartz aggregates being the most abundant form. Silicified serpentinites of Type II show extremely high values of silica (from 83 to 90 wt.% SiO_2) and low magnesium concentrations (from 4 to 8 wt.% MgO). Both types of silicified serpentinites have elevated content of REE and many other trace elements generally regarded as incompatible. We infer that the earlier silicification event was caused by the percolation of Si-rich hydrothermal fluids derived from igneous rocks, which intruded this area from ca. 380 to 330 Ma. A subsequent silicification event is the result of silica remobilization during intense chemical weathering under tropical conditions, which could have occurred between Late Cretaceous and Miocene.

Keywords: silicified serpentinites, silicification, serpentinized peridotites, cathodoluminescence imaging, Szklary Massif

1. Introduction

Silicification refers to the natural process in which primary mineral aggregates are replaced by various forms of crystalline and/or amorphous SiO_2. Silica is commonly derived from hydrothermal fluids that normally accompany volcanic activity (Gibson et al. 1983). On the other hand, supergene processes such as lateritic weathering can also be responsible for silica enrichment in certain horizons of lateritic regolith (Elias 2002; Butt, Cluzel 2013). Therefore, an increase in SiO_2 content can be triggered by many geological processes and chemical reactions, thus a universal silicification model does not exist. However, most of the previous studies have shown that silicified ultramafic rocks are products of broadly defined metasomatism or various types of supergene chemical weathering.

Strongly siliceous rocks referred to as birbirites have been previously described within ultramafic rocks in western Ethiopia (Duparc et al. 1927; Molly 1959) and in the Mauritanides Belts - the Gouérarate region (Moctar et al. 2019). According to the authors, the birbirites were formed by tropical weathering of dunites, which includes intense magnesium leaching simultaneously with silica recrystallization as secondary quartz and chalcedony. It was suggested by Moctar et al. (2019) that birbirites are a transitional lithology between unweathered peridotites (the protolith) and lateritic saprolite, which is the end-product of tropical weathering (Sherman et al. 1953). The term "silicified serpentinites" was used by Lacinska and Styles (2013) for rocks formed as a result of the incongruent dissolution of Mg-silicates followed by magnesium leach out and precipitation of microquartz (<20 μm spheroidal siliceous grains forming granular texture; e.g. Flörke et al. 1991). In this particular case, silicified serpentinites are considered as silcrete, corresponding to the residuum of palo-weathering surface. On the other hand, the hydrothermal origin of silicified serpentinites was proposed by Auclair et al. (1993) and was based on SiO_2-bearing hydrothermal fluids interaction with serpentinites. In this scenario, appreciable quantities of water and silica are liberated due to the transformation of serpentinites into talc-carbonate schists and lead to intense silicification of serpentinites which occurs at shallow depth. Serpentinites silicification, accompanied by listvenitization (the process of carbonate and silica alteration of mafic and ultramafic rocks; see e.g. Spiridonov 1991; Halls, Zhao 1995) have been reported within the Birjand ophiolite (Boskabadi et al. 2020). Silica listvenites (also called birbirites by the authors) are hosted, as smaller bodies, by other carbonate-rich listvenites, which confirms their relationship with these lithologies as well as their hydrothermal origin. Furthermore, thermodynamic models calculated by Klein and Garrido (2011) indicate that silicification of serpentinized peridotites is possible by fluid influx at a temperature below 200 °C.

In this article we present the results of the mineralogical and geochemical study of the silicified serpentinites from the Szklary Massif (southwestern Poland). These rocks contain various forms of silica together with different proportions of primary minerals typical for serpentinized peridotites. We therefore hypothesize that at least two different processes are responsible for the silicification of the studied ultramafic rocks.

2. Geological settings of the study area

Tectonically dismembered fragments of the Early Devonian oceanic lithosphere occur in the northeastern margin of the Bohemian Massif (Kryza, Pin 2010) (Fig. 1a). The obduction of oceanic crust and mantle rocks onto the continental margin is interpreted as a consequence of the Rheic Ocean closure during the Variscan multistage collision between Gondwana and Laurussia (Franke, Żelaźniewicz 2000; Mazur et al. 2006). Ultramafic and mafic rocks of the ophiolite sequence crop out as isolated massifs spread around the gneissic Góry Sowie Massif (Fig. 1b). All these massifs are collectively included in the so-called Central Sudetic Ophiolite (CSO) (e.g., Dubińska, Gunia 1997; Kryza, Pin, 2010; Awdankiewicz et al. 2021). Along the easter margin of the Góry Sowie Massif extends the Niemcza left-lateral shear zone (Mazur, Puziewicz 1995). This unit comprises mainly mylonitic gneisses accompanied by quartz-graphite schists, amphibolites, as well as undeformed Carboniferous syenites and diorites (Mazur, Puziewicz 1995; Pietranik et al. 2013). The Szklary Massif, also located within the Niemcza shear zone, is the smallest fragment of CSO (Fig. 1c).

The Szklary Massif is composed of weakly serpentinized peridotites including harzburgites and lherzolites, as well as a subordinate orthopyroxenites which are considered as lowermost fragment of the ophiolite sequence (Gunia 2000). Ultramafic rocks were affected by later metamorphism, particularly evident in the numerous shear zones, where primary minerals are replaced by chlorite-tremolite aggregates and Cr-spinel, talc, and actinolite as accessory minerals. Serpentinized peridotites from the Szklary Massif are often cut by narrow amphibolite veins enveloped by chlorite-rich zones, as well as different varieties of leucocratic rocks, including LCT-type pegmatites (Pieczka et al. 2019), aplites, and plagiogranites (Gunia 2007). Furthermore, lamprophyre dykes (kersantites and spessartites) (Niśkiewicz 1967) and rare metasomatic rocks such as rodingites can also be found (Dubińska et al. 2004). A distinctive feature of the Szklary Massif, which is not observed within other

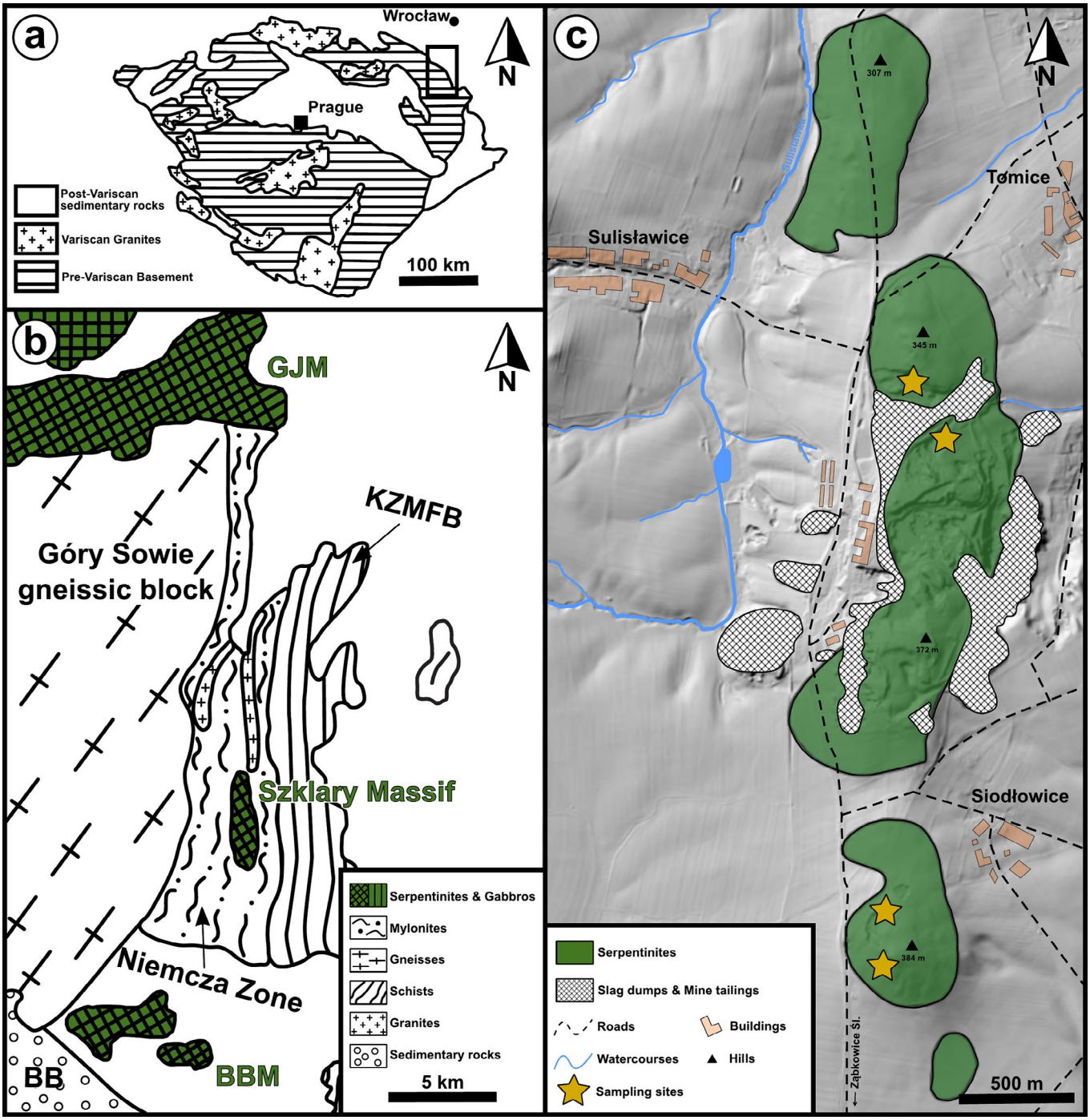

Figure 1. (a) Simplified sketch map of the Bohemian Massif (black rectangle represents the study area) and (b) western margin of the Góry Sowie block (modified after Aleksandrowski, Mazur 2002). (c) Geological map of the Szklary Massif (modified after Badura, Dziemiańczuk 1981). GJM – Gogołów-Jordanów Massif; KZMFB – Kamieniec Ząbkowicki Metamorphic Fold Belt; BBM – Braszowice-Brzeźnica Massif; BB – Bardo Basin. GJM, BBM and Szklary Massif are collectively termed as Central Sudetic Ophiolite (CSO).

CSO massifs, is the presence of a relatively thick lateritic cover (up to 76 m). It occurs in situ directly above unweathered serpentinized peridotite and forms a heterogeneous layer of saprolite with remnants of the parent rock, which marks the lowermost part of weathering profile (Dubińska et al. 2000; Niśkiewicz 2000). The lateritic cover consists mainly of partially or altered hydrous Mg-silicates, clay minerals, and a few varieties of silica, including rare gem-quality chrysoprase (green variety of chalcedony) (Čermáková et al. 2017). Elevated contents of dispersed iron oxides and oxyhydroxides are responsible for the distinctive reddish color. Moreover, some fragments of the saprolite layer contain abundant magnesite-quartz veins and are cut by numerous fractures mostly filled with amorphous silica together with greenish nickel-bearing clay minerals (Wiewióra, Szpila, 1975; Dubińska et al. 2000). Most of the previous studies of the lateritic cover from the Szklary Massif were based on core samples obtained during local drilling projects. These revealed the presence of strongly siliceous and

porous metasomatic rock (e.g., Niśkiewicz 2000; Mikulski 2014). On the grounds of chemical and physical similarities to Ethiopian birbirites, Mikulski (2014) stated that this horizon enriched in silica developed due to intense chemical weathering and seasonal groundwater fluctuations under subtropics climate conditions. This led to chemical elements migration within saprolite triggered by changes in the pH-Eh conditions. Intense silica enrichment and its recrystallization combined with simultaneous loss of elements such as Mg, Ni, Cr, and Co suggest that the birbirite from the Szklary region is a product of near-surface processes (Mikulski 2014).

3. Analytical methods

During the field work 32 samples were collected. They represent various rock types, but predominantly serpentinized peridotites and silicified serpentinites, as well as solid and loose lateritic material from the saprolite horizon. The bulk-rock chemistry of samples was analyzed in the laboratories of Bureau Veritas Minerals (Vancouver, Canada). Silicified serpentinites, partially serpentinized peridotites, and hard saprolite were analyzed by inductively coupled plasma mass spectrometry (ICP-MS), following the fusion of samples in lithium borate. The method reproducibility (2SE) assessed by replicates ranges from 0% (CaO) to 1.6% (Cr_2O_3) at 95% confidence limits. Analytical accuracy (2SE) based on measurements of 4 standard STD SO-19 is from 0.25% (Al_2O_3) to 4.4% (Ba) at 95% confidence limits. Moreover, the chemical composition of loose saprolite was determined by X-ray fluorescence (XRF) analysis. The preparation procedure consisted of samples fusion in a platinum gold crucible with a lithium tetraborate flux followed by casting into a disc to lower the negative impact of moisture accumulation and obtain a better quality of analyses. The method reproducibility (2SE) assessed by replicates is below 1% for major elements, as well as nickel and commodity elements for nickeliferous laterites; 0.8% (Ni) and 8.3% (Co) at 95% confidence limits. For XRF analysis, analytical accuracy, as estimated from the real concentration in the standard STD OREAS 184 is below 1% for major elements, as well as nickel and cobalt. Petrographic thin sections were studied using an optical microscope (Zeiss Axioskop EL-Einsatz) and scanning electron microscope JEOL JSM-IT100 (SEM-EDS) equipped with monochromatic cathodoluminescence detector Deben Centaurus (SEM-CL). For complete information about crystalline phases identification of silicified serpentinites and accompanying rocks, manually ground samples were examined using X-Ray diffraction (XRD). Measurements were performed on Bruker D8 ADVANCE diffractometer with CuKα radiation (1.5406 Å), counting time 1.9° 2θ/min and 3° - 75° 2θ range. For qualitative differentiate mineral phases, we used the DIFFRAC.EVA software with PDF - 4+ database. Electron and optical microscope investigations, as well as X-Ray diffraction analyses were carried out at the Institute of Geological Sciences (University of Wrocław).

4. Field observations

Natural outcrops of silicified serpentinites have not been documented in the northern part of the Szklary Massif, therefore only single blocks of rusty and porous quartzitic rocks were collected on the field. The situation is different in the central and southern parts of the Szklary Massif, where new outcrops of silicified serpentinites have been documented during fieldwork. Silicified zones crop out within serpentinized peridotites (Fig. 2a) and overlying lateritic cover (Fig. 2b). They usually form relatively narrow vertical or subvertical elongated

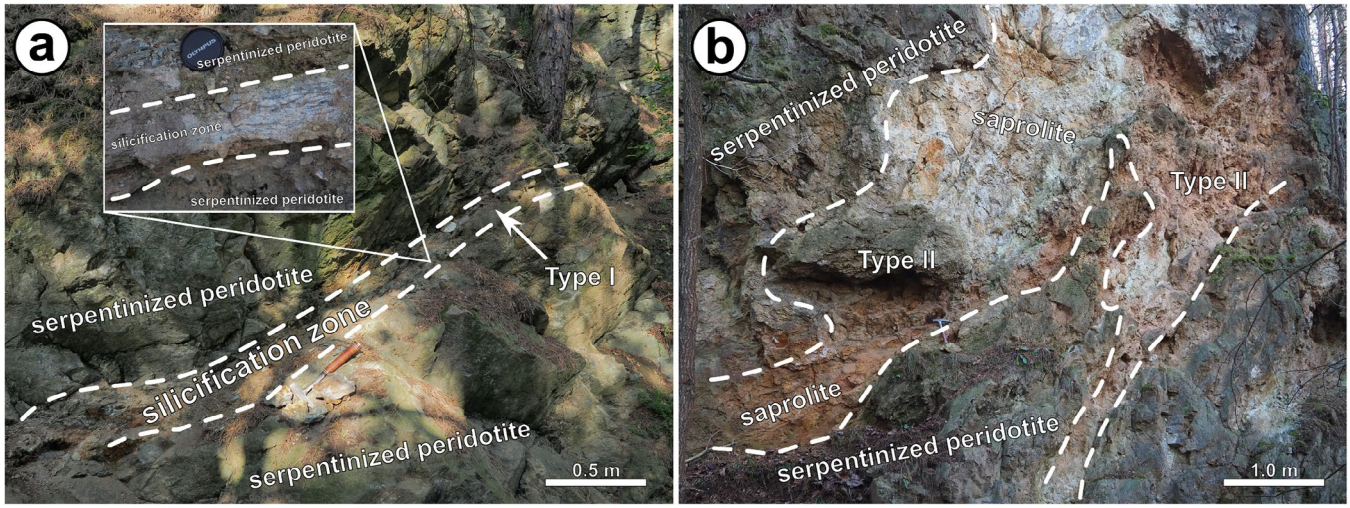

Figure 2. (a) Field photos showing silicification within serpentinized peridotites – Type I. Inset shows contact between serpentinized peridotite (host rock) and silicification zone. (b) Silicified zones located within lowermost part of the saprolite horizon – Type II.

zones, occasionally similar in shape to the convex lens. Silicified zones located above and beneath the weathering front demonstrate slightly different macroscopic features. Two types of silicified serpentinites, hereafter referred to as Type I and Type II, have been already distinguished during fieldwork (Fig. 3). Major differences are manifested by the presence of primary minerals and iron oxyhydroxide, resulting in changes of color tone already at the outcrop scale. Type I represents silicified serpentinites collected mainly from horizontally elongated zones, surrounded by serpentinized peridotites, beneath the lateritic cover. It contains more primary minerals representative for serpentinites and it is usually less weathered and porous. Moreover, Type I contains either quartz or chalcedony veinlets oriented in a comparable direction. Type II crops out within the saprolite zone, which is situated directly above serpentinized peridotites. It is more porous and does not contain visible primary minerals except for corroded grains of Cr-magnetite. Type II is noticeably harder and more silicified than Type I. The samples of Type II display intense rusty color, and the pores are occasionally filled up by quartz and colorless opal.

5. Petrography and chemical composition of silicified serpentinites

5.1. Type I

Silicified serpentinites have been divided into two main types according to their textural and optical properties. The differences in chemical and mineral composition between the types are also consistent with this division. Macroscopically, Type I displays a cryptocrystalline texture, but a minor amount of serpentine minerals and single grains of Cr-magnetite remain visible by the unaided eye. Microscopic examination revealed that primary minerals are mostly well preserved, as well as light color veinlets filled with microscale quartz clusters alternating with minor amounts of cryptocrystalline silica (Fig. 4a). Relicts of the original mineralogy are recognizable in thin sections. They are represented by amphiboles, which appear as bladed and/or acicular crystals, as well as Cr-magnetite represented by irregular-shaped, opaques grains. Relicts of serpentine and clinochlore usually display pale green color. They appear as parallel fibers or asbestiform crystals (serpentine) and tabular crystals characterized by perfect cleavage (clinochlore). Qualitative analysis, obtained from X-ray diffraction and SEM-EDS, revealed the presence of talc, tremolite and anthophyllite. Further observation of backscattered electron (BSE) images obtained from Type I have shown that the most striking feature is the presence of numerous veinlets overgrown by euhedral quartz crystals. Preserved rock-forming silicates are usually cut by these veinlets (Fig. 4b). Moreover, in studied veinlets, single zircon grains (<20 μm) were observed as inclusions (Fig. 4c), as well as alkali feldspar but in this particular case the chemical analysis is uncertain due to the extremely small size of the grain (<10 μm). Quartz crystals occurring within the veinlets display characteristic oscillatory zoning under cathodoluminescence (Fig. 4d). A minor amount of chalcedony and microquartz grains have been documented in some parts of studied Type I where primary minerals. In comparison to protolith, samples of silicified serpentinites (Type I) are generally enriched in Si (from 63 to 69 wt.% SiO_2) and depleted in Mg (from 10 to 19 wt.% MgO). All samples of Type I show elevated K_2O content and two samples are characterized by Al_2O_3 concentration higher than average for serpentinized peridotites (Fig. 5). Other major oxides concentrations are roughly the same as measured in partially serpentinized peridotites (Table 1). Silicified serpentinites (Type I) show elevated concentrations of rare-earth elements (REE), whereas in serpentinized peridotites abundances of these elements are usually below the detection limits. Moreover,

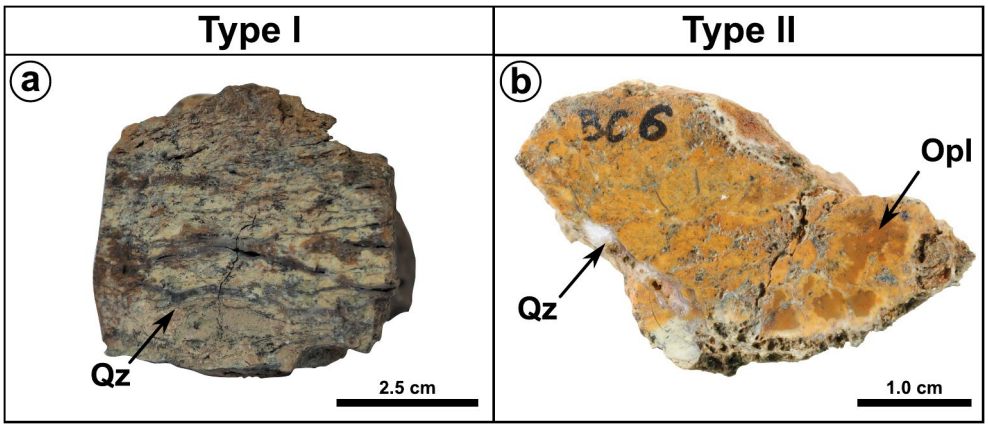

Figure 3. Examples of silicified serpentinites occurring within the Szklary Massif. (a) Type I is less weathered and porous and usually display grayish color. Note that quartz veinlets (Qz) are oriented roughly in one direction. (b) Type II is characterized by rusty orange color, as well as presence of pores and colorless opal (Opl).

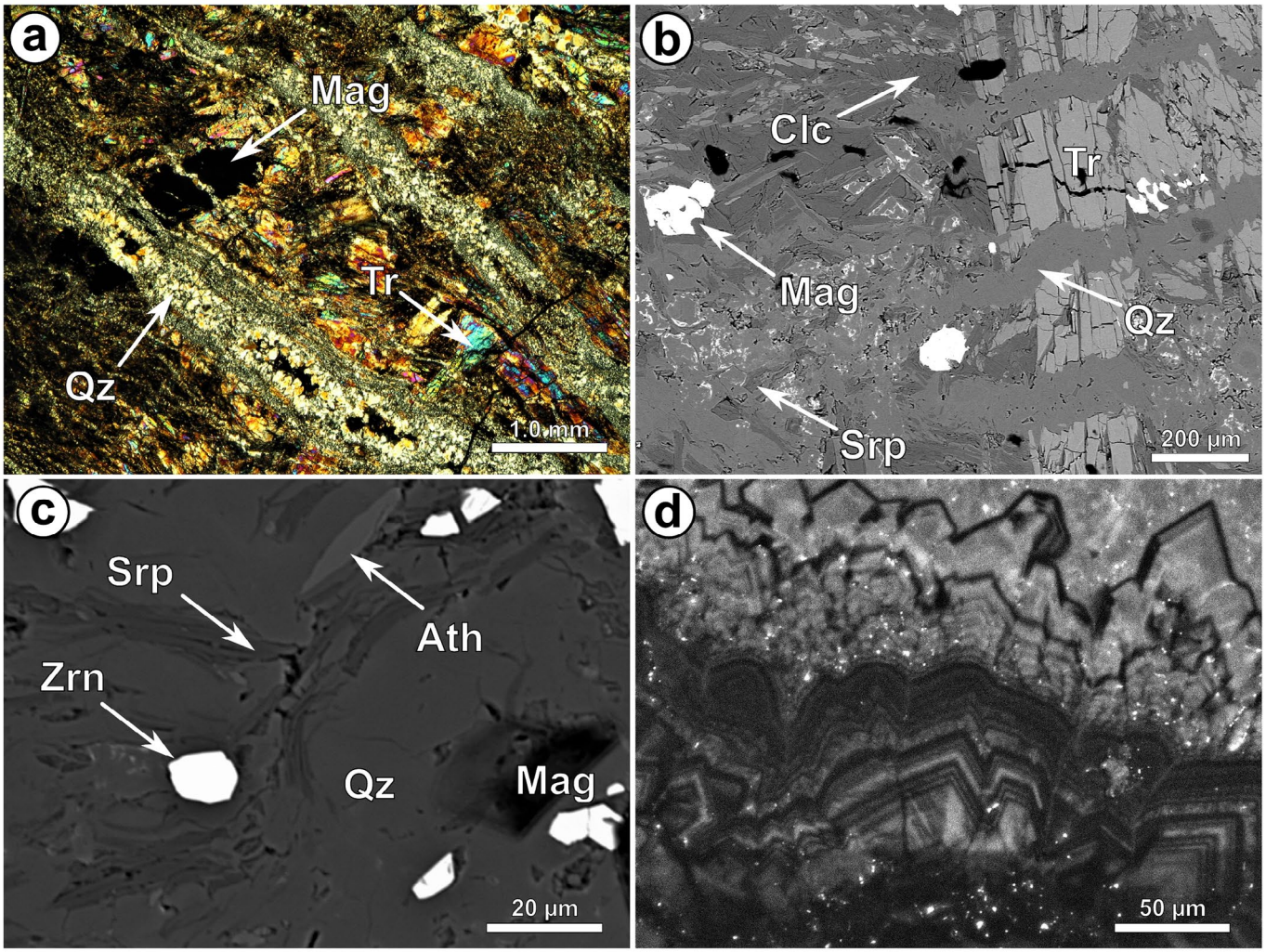

Figure 4. Microscopic (a), back-scattered electron (b, c) and cathodoluminescence (d) images of the silicified serpentinite (Type I). (a) Primary tremolite aggregates (Tr) and magnetite grain (Mag) invaded by a late quartz veinlet (Qz). (b) Tremolite crystal cut by a silica veinlets (Qz). The groundmass of Type I is mostly composed of cryptocrystalline silica intermixed with relicts of serpentine (Srp), clinochlore (Clc) and subhedral magnetite grains (Mag). (c) Zircon grain (Zrn) enveloped by quartz (Qz) and anthophyllite (Ath) and serpentine (Srp) aggregates. (d) Euhedral growth zones of hydrothermal vein quartz.

samples representing ultramafic rocks are characterized by comparable Co and Ni compositions, while in Type I samples these elements are more variable. Also, Rb and Y concentrations measured in Type I are enriched in comparison to the protolith (Fig. 6). Complete trace element compositions of the studied samples are reported in Table 2.

5.2. Type II

The characteristic textural feature of Type II is the presence of partially porous zones, manifested by circular and oval-shaped vesicles whose diameter is up to 1mm (Fig. 7a). The distribution of porous zones is irregular and they often border with massive parts. Type II displays an almost homogeneous intense rusty orange color. Macroscopically, the groundmass of rock is mostly indistinguishable, except for colorless opal, as well as milky and transparent silica veins, which thickness usually does not exceed 1 cm. In thin section, the groundmass of Type II is mainly composed of non-crystalline silica aggregates which often mimic the original mesh texture of serpentinized peridotite (Fig. 7b). Strongly corroded and subangular Cr-magnetite grains are also recognizable. Veins with euhedral quartz are present but less common in Type II (Fig. 7c). The non-crystalline silica aggregates, which are the most common component of the groundmass, are strongly intermixed with opaque and deep-red brown iron oxyhydroxides. This particular feature makes thin sections of Type II difficult to examine under the petrographic microscope, because iron oxyhydroxides mask the optical properties of preserved minerals. However, further SEM-BSE observations of Type II revealed that the groundmass is mostly occupied by so-called microquartz grains which usually form larger clusters (Fig. 7d). Relics of talc, bladed tremolite and fibrous serpentine minerals were observed in interstices between the microquartz grains. Moreover, qualitative XRD analysis revealed the presence of clinochlore. Type II is characterized by extremely high silica (from 83

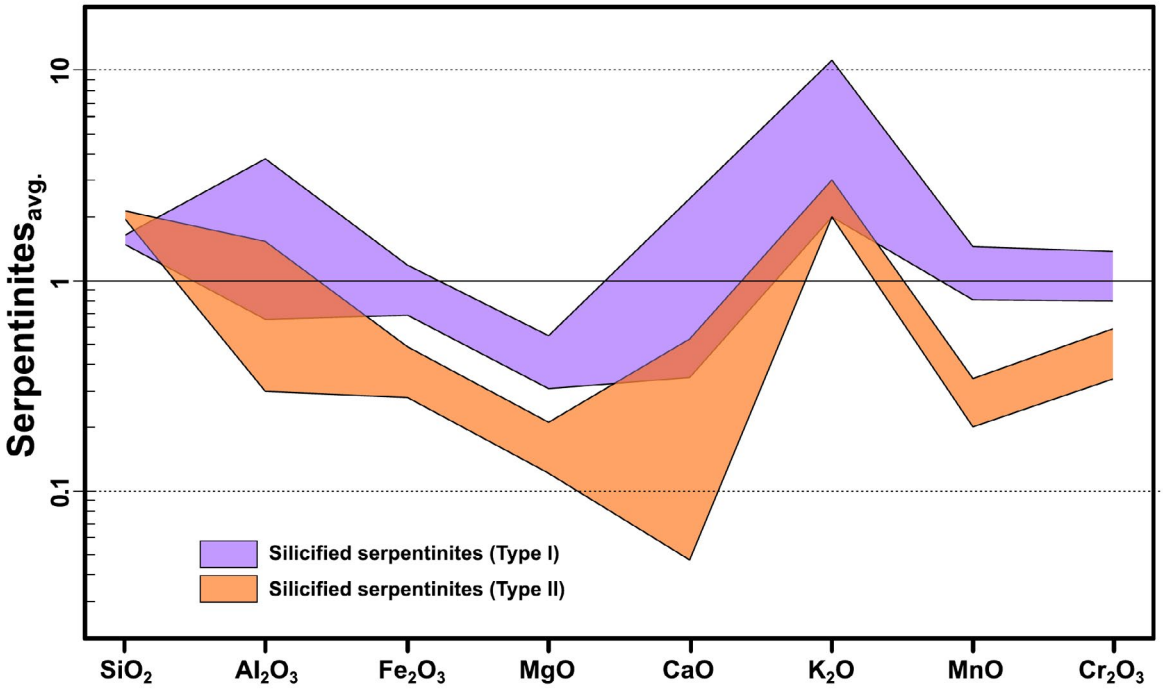

Figure 5. Major oxides composition of two types of silicified serpentinites. The value '1' corresponds to the average composition of partially serpentinized peridotites from the Szklary Massif (see Table 1).

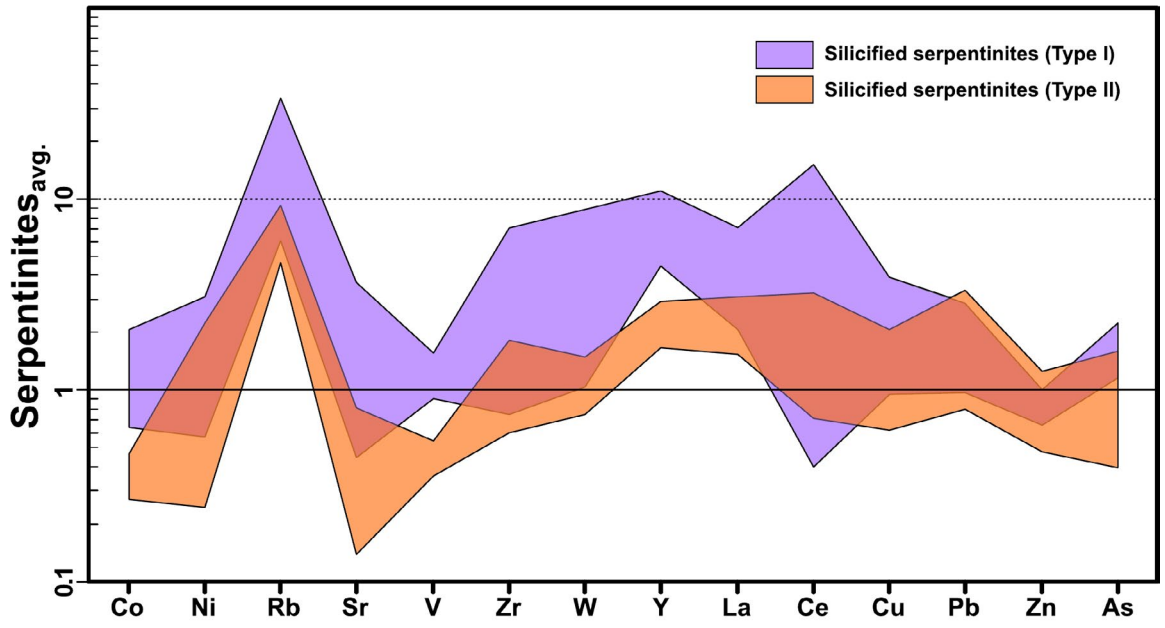

Figure 6. Trace element compositions of two types of silicified serpentinites. The value '1' corresponds to the average composition of partially serpentinized peridotites from the Szklary Massif (see Table 2).

to 90 wt.% SiO_2) and low magnesium values (from 4 to 8 wt.% MgO). In comparison to the protolith, the chemical analyses showed a slightly lower content of Fe (up to 5 wt.% Fe_2O_3), as well as CaO (up to 0.7 wt.%), MnO (up to 0.05 wt.%) and Cr_2O_3 (up to 0.32 wt.%) (Fig. 5). Other major oxides present comparable values (Table 1). Unlike serpentinized peridotites, the concentrations of REE in silicified serpentinites of Type II are usually above detection limits (Table 2). In comparison with the ultramafic protolith, all samples representing Type II are depleted in Co, while Ni shows a range of concentrations. Moreover, Rb and Y concentrations are higher, while V and Sr display lower concentrations than in the protolith (Fig. 6).

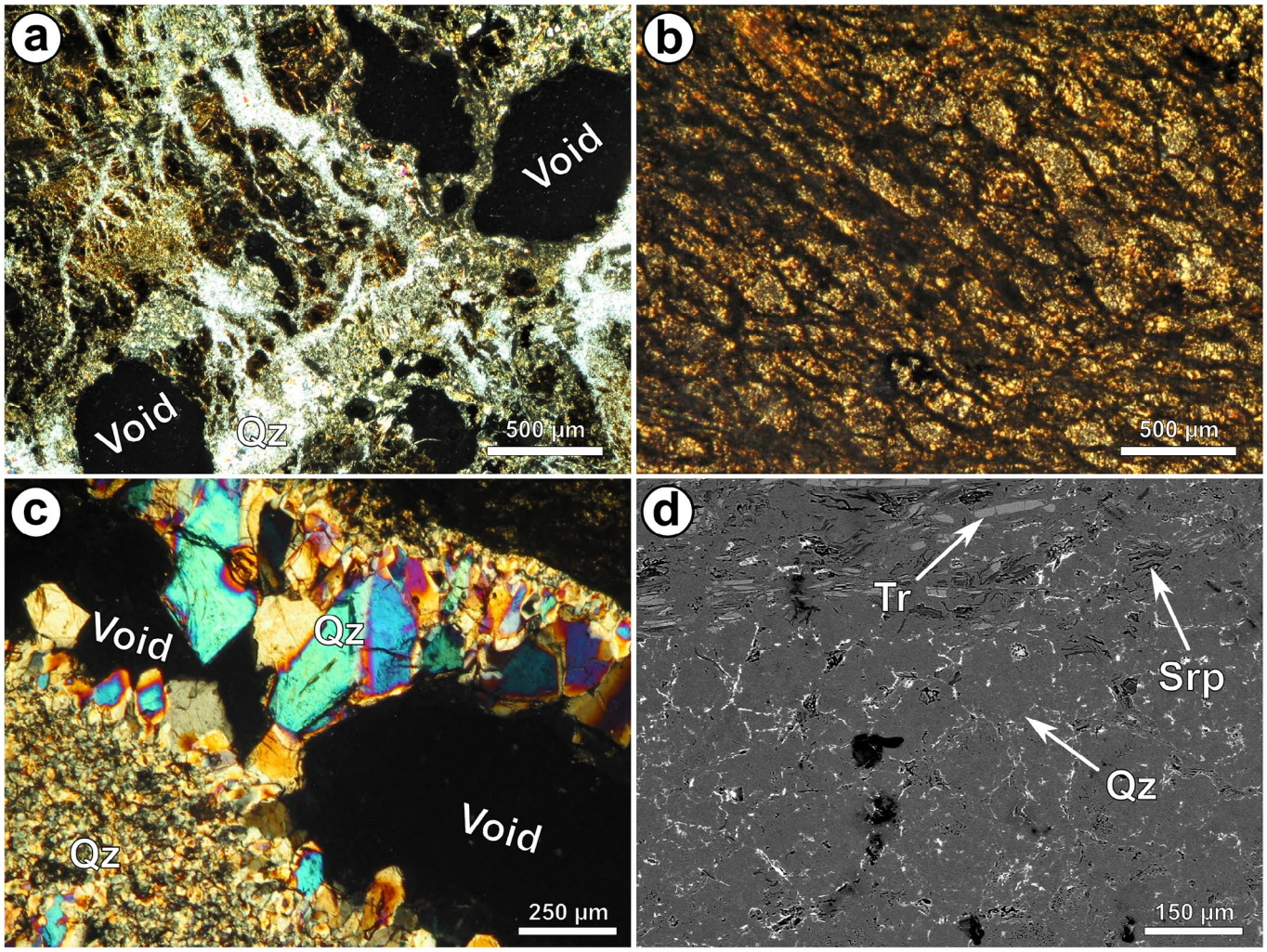

Figure 7. Microscopic (a, b, c) and back-scattered electron (d) images of the silicified serpentinite (Type II). (a) Characteristic porous texture of Type II. Between single voids occur numerous quartz veinlets (Qz). (b) Microquartz aggregates form pseudomorphs after primary minerals and mimic mesh texture of partially serpentinized peridotites. (c) Vein with euhedral quartz (Qz). Note that the quartz crystals grow toward the central part of void. (d) Spheroidal microquartz grains (Qz) and relicts of primary minerals, tremolite (Tr) and serpentine (Srp).

6. Discussion

6.1. Petrography of silicified serpentinites

Petrographic studies on silicified serpentinites from the Szklary Massif revealed that these rocks are mainly composed of different types of silica. In samples representing silicified serpentinites of Type I the groundmass is composed of numerous veinlets, mainly filled with quartz clusters and minor amounts of cryptocrystalline silica. Nevertheless, the presence of various silica forms is not as abundant as in Type II. Additionally, the most striking feature of Type I is well-preserved primary minerals, whereas Type II is characterized by an almost complete lack of primary minerals other than silica. This difference is probably caused by uneven dissolution of Mg-silicates within the lower zones of the lateritic profile, especially on the boundary between parent rock and saprolite, where fluid circulation could be not as pervasive as within the subsurface horizons. According to Golightly (2010), limited drainage within the saprolite zone enhances the process of silica precipitation and deposition. Microscale structural analyses of Type I reveal the presence of numerous veinlets filled with quartz crystals. Their spatial and geometric configuration in oriented samples mimics the elongation trend of silicification zones. This may suggest that Si-rich fluid flow occurred only in certain well-defined directions. Quartz crystals occurring in Type I display a few textural variations, nevertheless the most common texture could be described as euhedral growth zones of oscillating cathodoluminescence intensity (Rusk 2012). These CL signatures indicate hydrothermal rather than weathering origin of quartz crystals occurring in silicified serpentinites of Type I (Götte et al. 2011; Rusk 2012; Frelinger et al. 2015). According to Rusk (2012), the correlation between the properties of quartz growth zones and crystallization temperature is uncertain. However, euhedral and well-formed crystals are generally considered to be derived from low temperature and/or epith-

Table 1. Average major oxides composition of previously studied silicified ultramafic rocks and major oxides composition of investigated types of silicified serpentinites and serpentinized peridotites from the Szklary Massif.

wt.%	SiO_2	Al_2O_3	Fe_2O_3	MgO	CaO	K_2O	MnO	Cr_2O_3	LOI	Total
	Serpentinized peridotites									
BC2	39.67	0.68	8.39	37.28	0.48	<0.01	0.12	0.37	12.70	99.69
BC3	44.59	0.87	9.36	30.74	1.89	<0.01	0.13	0.37	11.70	99.65
BC4	41.46	1.12	8.20	35.47	0.99	<0.01	0.12	0.30	12.00	99.66
BC15	42.82	0.73	9.12	33.72	1.46	<0.01	0.13	0.47	11.20	99.65
BC17	42.02	1.14	9.08	37.31	0.10	<0.01	0.12	0.35	9.60	99.72
BC22	39.91	0.71	9.21	39.35	0.17	<0.01	0.12	0.38	9.80	99.65
Avg.	41.75	0.88	8.89	35.65	0.85	<0.01	0.12	0.37	11.17	
	Silicified serpentinites (Type I)									
BC10	62.62	0.59	7.33	19.60	0.47	0.02	0.10	0.37	8.50	99.60
BC12*	68.74	3.34	10.49	9.89	0.34	0.12	0.18	0.51	4.40	98.00
SS1	68.00	2.06	6.56	12.65	2.29	0.02	0.10	0.30	7.70	99.68
BC21	69.36	0.40	8.99	12.52	0.16	0.02	0.11	0.58	7.40	99.54
	Average composition of silica-carbonate listvenites [(1), (2)]									
	45.39	0.91	4.84	19.62	4.82	0.58	0.09	-	22.6	
	Silicified serpentinites (Type II)									
BC6	88.26	0.51	3.24	4.57	0.69	0.02	0.04	0.13	2.30	99.76
BC9	89.80	0.37	2.47	4.30	0.37	0.02	0.03	0.11	2.30	99.77
BC16	82.54	1.55	4.34	7.30	0.64	0.02	0.02	0.32	2.80	99.53
BC19	84.22	0.48	2.92	7.53	0.03	0.02	0.05	0.10	4.00	99.35
BC20	86.69	0.26	3.45	5.58	0.06	0.03	0.02	0.09	3.70	99.88
	Average composition of silica listvenites [(1)], birbirites [(2), (3)] and silicified serpentinites [(4)]									
	84.5045	0.78667	6.7185	1.567	2.10842	0.11833	0.07	0.43	4.01	

*The chemical composition of sample BC12 is derived from the XRF analysis; <0.1 – values indicating detection limits

(1) Boskabadi et al. (2020)

(2) Gahlan et al. (2020)

(3) Mikulski (2014)

(4) Lacinska, Styles (2013)

ermal environments (<300ºC) (Dong et al. 1995; Götze 2009). Unweathered primary minerals are irregularly cut by silica veinlets and somewhat less often along their cleavage planes. The presence of sharp contact between silica and primary phases and lack of reaction zones may indicate that fluid influx was relatively rapid. Further BSE observations revealed the occurrence of zircon inclusions within silica veinlets. Zircon is probably not an authigenic component of partially serpentinized peridotites from Szklary Massif, whereas hydrothermal origin, related to the presence of Si-rich fluids, is theoretically possible. However, due to the small size of grains (<20 μm), the characteristic textural features of the hydrothermal zircon have not been observed in our samples (Schaltegger 2007). At present, we assume that zircon was relocated from another geological environment and subsequently emplaced within serpentinized peridotites, together with Si-rich fluid.

Type II is characterized by a random distribution of various forms of silica, however the groundmass composition is predominantly occupied by microquartz aggregates, with minor silica veinlets similar to those in Type I. A comprehensive mechanism of microquartz formation within ultramafic rocks was proposed by Lacinska and Styles (2013). Incongruent in situ dissolution of Mg-silicates occurs in the phreatic zone, where meteoric and groundwater fluids mingle with each other. This leads to the formation of an environment characterized by near-neutral pH, which is favorable to microquartz, as well as opal precipitation from a fluid. The silicification model presented by Lacinska and Styles (2013) is similar to the hypothesis formulated by Mikulski (2014), who proposed that silicification of ultramafic rocks in Szklary was possible due to silica recrystallization and intense leaching of Mg within zone characterized by fluctuations of the groundwater table. The resemblance in high silica

Table 2. Trace elements composition of investigated types of silicified serpentinites and serpentinized peridotites from the Szklary Massif.

	Serpentinized peridotites							Silicified serpentinites (Type I)				Silicified serpentinites (Type II)				
ppm	BC2	BC3	BC4	BC15	BC17	BC22	avg.	BC10	BC12*	SS1	BC21	BC6	BC9	BC16	BC19	BC20
Co	116.2	123.7	116.7	120.4	113.8	123.4	119	98	248.6	69.9	115.8	53.6	32.3	41.4	55.2	31.8
Ni	2054	2165	2271	2343	2036	2386	2209	2534	6760	1021	1995	1410	1252	1886	4954	536
Cs	<0.1	1	0.4	<0.1	<0.1	<0.1	0.7	3	3.2	0.9	2.3	1.4	1.7	0.7	2.2	2.6
Ga	<0.5	<0.5	<0.5	<0.5	0.9	<0.5	0.9	<0.5	2.6	3.3	<0.5	1.2	<0.5	<0.5	<0.5	<0.5
Hf	<0.1	<0.1	<0.1	<0.1	<0.1	<0.1	<0.1	<0.1	0.1	0.1	<0.1	<0.1	<0.1	<0.1	<0.1	<0.1
Nb	<0.1	<0.1	<0.1	<0.1	<0.1	<0.1	<0.1	<0.1	0.6	0.3	<0.1	0.8	0.1	0.2	<0.1	<0.1
Rb	<0.1	0.7	0.2	0.1	0.2	<0.1	0.3	2.6	10.2	1.5	2.8	2	1.6	1.4	2.1	2.8
Sn	<1	<1	<1	<1	7	<1	7	<1	<1	<1	<1	<1	<1	<1	<1	<1
Sr	2.3	6.7	5.1	4.5	1.3	1.7	3.6	1.6	3.2	13.3	1.9	2.3	1.6	2.9	0.5	0.9
Ta	<0.1	<0.1	<0.1	<0.1	<0.1	<0.1	<0.1	<0.1	<0.1	<0.1	<0.1	<0.1	<0.1	<0.1	<0.1	<0.1
Th	<0.2	<0.2	<0.2	<0.2	<0.2	<0.2	<0.2	<0.2	0.9	0.4	<0.2	<0.2	<0.2	<0.2	<0.2	<0.2
U	<0.1	<0.1	<0.1	<0.1	<0.1	<0.1	<0.1	1.1	0.4	0.3	0.6	<0.1	<0.1	0.3	0.3	0.3
V	41	44	36	49	43	40	42.17	40	66	35	51	18	17	25	15	18
W	<0.5	<0.5	<0.5	0.5	0.6	0.9	0.67	<0.5	0.7	<0.5	1.6	1	0.6	1	0.5	0.9
Zr	0.4	0.4	0.4	0.3	1.9	0.6	0.67	0.9	5.6	3.6	0.5	2.1	0.8	1.2	0.4	0.7
Y	0.1	0.3	0.1	0.2	0.2	0.2	0.18	0.7	2	1	1.3	0.6	0.3	0.6	0.3	0.3
La	0.4	0.5	0.7	0.5	1.1	0.3	0.58	1.6	4.1	1.3	1.2	1.8	0.9	1.3	1.3	1.1
Ce	0.2	0.4	0.2	<0.1	0.5	0.1	0.28	0.2	4.7	1	0.1	0.4	0.2	0.9	0.2	0.2
Pr	<0.02	0.02	<0.02	<0.02	0.04	<0.02	0.03	0.19	0.69	0.22	0.18	0.12	0.06	0.18	0.11	0.04
Nd	<0.3	<0.3	<0.3	<0.3	<0.3	<0.3	<0.3	0.7	2.6	0.9	0.9	0.4	0.3	0.7	0.5	0.3
Sm	<0.05	<0.05	<0.05	<0.05	<0.05	<0.05	<0.05	0.11	0.49	0.18	0.26	0.07	<0.05	0.09	<0.05	<0.05
Eu	<0.02	<0.02	<0.02	<0.02	<0.02	<0.02	<0.02	0.04	0.11	0.04	0.03	<0.02	<0.02	0.03	<0.02	<0.02
Gd	<0.05	<0.05	<0.05	<0.05	<0.05	<0.05	<0.05	0.09	0.46	0.15	0.29	0.13	0.06	0.12	<0.05	0.06
Tb	<0.01	<0.01	<0.01	<0.01	<0.01	<0.01	<0.01	0.01	0.07	0.02	0.05	0.01	<0.01	0.02	<0.01	0.01
Dy	<0.05	<0.05	<0.05	<0.05	0.05	<0.05	0.05	0.06	0.4	0.15	0.26	0.07	<0.05	0.11	<0.05	0.06
Ho	<0.02	<0.02	<0.02	<0.02	<0.02	<0.02	<0.02	0.02	0.07	0.03	0.05	0.02	<0.02	0.03	<0.02	<0.02
Er	<0.03	0.04	<0.03	<0.03	<0.03	0.03	0.035	0.07	0.22	0.1	0.14	0.07	0.03	0.06	<0.03	0.03
Tm	<0.01	<0.01	<0.01	<0.01	<0.01	<0.01	<0.01	<0.01	0.03	0.01	0.01	0.01	<0.01	<0.01	<0.01	<0.01
Yb	<0.05	<0.05	<0.05	<0.05	<0.05	<0.05	<0.05	0.08	0.25	0.1	0.09	0.06	<0.05	0.08	<0.05	0.08
Lu	<0.01	0.01	<0.01	<0.01	<0.01	<0.01	0.01	<0.01	0.04	0.02	0.02	0.01	<0.01	<0.01	<0.01	0.01
Mo	<0.1	<0.1	<0.1	<0.1	<0.1	<0.1	<0.1	<0.1		<0.1	<0.1	0.2	0.1	0.1	<0.1	0.2
Cu	5.6	0.8	1.2	1.6	4.3	1	2.42	2.9		9.4	2.3	3.3	1.8	4.3	1.5	5
Pb	0.9	0.4	0.3	1.8	0.2	0.2	0.63	1		0.6	1.8	1.2	1	1.3	0.5	2.1
Zn	28	26	32	35	26	26	28.83	27		17	29	25	14	36	21	13
As	<0.5	1.9	2	1.8	0.9	1.6	1.64	1.9		<0.5	3.7	0.8	0.6	0.6	0.8	3
Cd	<0.1	<0.1	<0.1	<0.1	<0.1	<0.1	<0.1	<0.1		<0.1	<0.1	0.1	0.1	0.1	0.3	<0.1
Sb	<0.1	<0.1	<0.1	<0.1	<0.1	0.1	0.1	0.1		<0.1	0.3	<0.1	<0.1	<0.1	<0.1	0.5
Bi	<0.1	<0.1	<0.1	<0.1	<0.1	<0.1	<0.1	<0.1		<0.1	<0.1	<0.1	<0.1	<0.1	<0.1	<0.1
Ag	<0.1	<0.1	<0.1	<0.1	<0.1	<0.1	<0.1	<0.1		<0.1	<0.1	<0.1	<0.1	<0.1	<0.1	<0.1
Au	<0.5	<0.5	<0.5	<0.5	0.9	<0.5	0.9	1.2		0.9	<0.5	<0.5	<0.5	1.1	<0.5	<0.5
Hg	0.01	<0.01	<0.01	<0.01	<0.01	<0.01	0.01	0.03		0.03	0.06	0.01	<0.01	0.02	<0.01	0.03
Tl	<0.1	0.1	<0.1	<0.1	<0.1	<0.1	0.1	<0.1		<0.1	<0.1	<0.1	<0.1	<0.1	<0.1	<0.1
Se	<0.5	<0.5	<0.5	<0.5	<0.5	<0.5	<0.5	<0.5		<0.5	<0.5	<0.5	<0.5	<0.5	<0.5	<0.5

*The chemical composition of sample BC12 is derived from the XRF analysis; <0.1 – values indicating detection limits

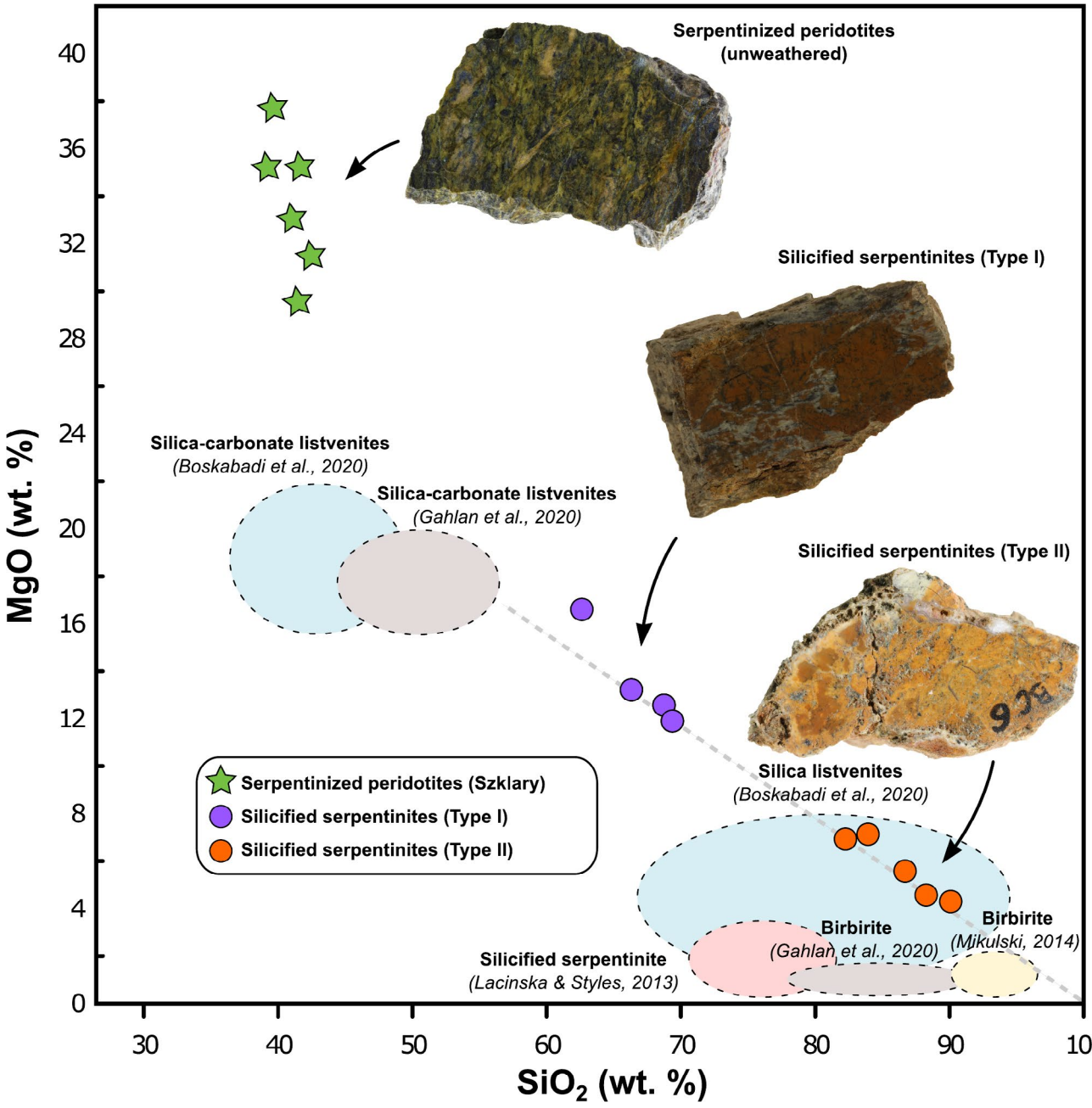

Figure 8. Whole-rock SiO_2 vs. MgO chemical composition of the silicified serpentinites and serpentinized peridotites from the Szklary Massif, compared with field boundaries representing the chemical composition of silica-carbonate listvenites (Boskabadi et al. 2020; Gahlan et al. 2020), silica listvenites (Boskabadi et al. 2020), silicified serpentinites (Lacinska, Styles 2013) and birbirites (Mikulski 2014; Gahlan et al. 2020). Average major oxides composition of previously studied silicified ultramafic rocks are presented in Table 1.

content (from 89 to 94 wt.% SiO_2), intense decomposition of the magnesium silicates, as well as macroscopic features, such as numerous pores and rusty color suggest that rocks described as birbirite by Mikulski (2014) could be the analogs of rocks described as silicified serpentinites of Type II in this study. The microquartz patterns which mimic the mesh texture of partially serpentinized peridotite suggest that roundish silica aggregates are the residue after olivine dissolution (Fig. 7b, d). Aggregates that form pseudomorphs after serpentine or tremolite occur less frequently, which indicates that chemical disintegration was more intense for olivines than for other rock-forming silicates. Silica veinlets occurring in Type II are mostly filled with a cryptocrystalline form of silica whereas euhedral quartz crystals are less widespread than in silicified serpentinites of Type I. Therefore, considering previous studies (Mikulski 2014), as well as mechanisms of the silica remobilization associated with the intense removal of the alkaline earth metals during the ultramafic rocks lateritization (Golightly 2010; Butt, Cluzel 2013; Lacinska, Styles 2013), we suggest that chemical weathering under tropical conditions was the primary cause of Type II silicification.

Different intensity of water drainage conditions at the boundary between the lowermost saprolite and ultramafic bedrock could be essential for the diversity of

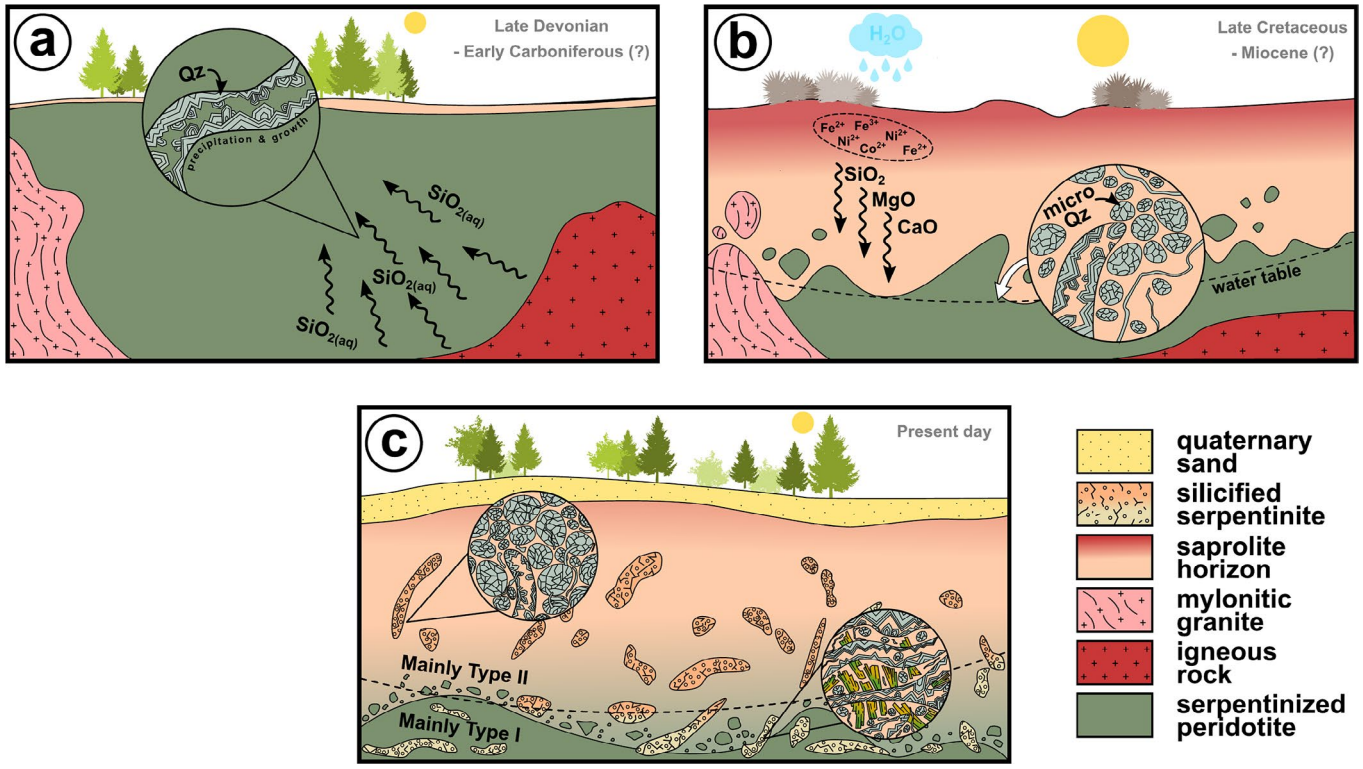

Figure 9. Simplified sketch showing the probable sequence and timing of the silicification processes within serpentinized peridotites from the Szklary Massif. (a) Precipitation and growth of euhedral quartz crystals, caused by Si-rich hydrothermal fluid influx into serpentinized peridotites. The presence of enriched in silica hydrothermal fluid is most likely related to Late Devonian – Early Carboniferous magmatism. (b) Silica remobilization and microquartz precipitation caused by intense tropical weathering between Late Cretaceous and Miocene. (c) Present situation that reflects the results of two different silicification processes. Note that silicified serpentines of Type I occur mostly within serpentinized peridotites, whereas Type II usually occur within saprolite horizon.

studied silicified serpentinites. The most intensive silica precipitation and replacement of Mg-silicates occurred within the bottom of the saprolite horizon. This is mainly manifested by the presence of microquartz aggregates mimicking the original mesh texture of the protolith. Petrographical analyses show that this feature is more common in silicified serpentinites of Type II. However, if serpentinized peridotite had been locally affected by hydrothermal fluid before primary minerals dissolution, the newly formed silicified serpentinites would contain hydrothermal quartz (earlier generation), as well as minor amounts of weathering silica and microquartz (later generation). In this study, we infer that the presence of both silica generations is a characteristic feature for silicified serpentinites described as Type I.

6.2. Geochemical implications

Nearly all serpentinized peridotites are mainly composed of SiO_2, MgO and H_2O, where water is embedded in serpentine minerals (Coleman 1971). Geochemical analysis of partially serpentinized peridotites from the Szklary Massif showed that silica content varies from 40 to 45 wt.% SiO_2 and the magnesium content varies from 31 to 39 wt.% MgO (Table 1). Additionally, in analyzed samples Fe_2O_3 content does not exceed 10 wt.% and loss on ignition (LOI) varies from 10 to 13 wt.%, which indicates that the studied samples are relatively unweathered. Thus, we presume that changes in MgO/SiO_2 ratios do not reflect the degree of rock decomposition, but are rather related to the primary proportion between the main rock-forming minerals, such as olivines, tremolite and serpentine minerals. Representative samples of unweathered serpentinized peridotites have 37-39 wt.% MgO, while serpentinized peridotites, classified as partially weathered have approx. 31 wt.% MgO. Samples representing both types of silicified serpentinites are significantly enriched in silica and depleted in magnesium with varying degrees of intensity (Fig. 8).

The silica content in silicified serpentinites of Type I is higher than in serpentinized peridotites and does not clearly overlap with silica-carbonate listvenites (e.g., Boskabadi et al. 2020; Gahlan et al. 2020). Although the MgO concentrations are comparable in both groups of rocks, Type I does not contain minerals typical for silica-carbonate listvenites, such as euhedral magnesite, dolomite, calcite, Cr-rich muscovite, sulfides, and native gold (Aftabi, Zarrinkoub, 2013; Gahlan et al. 2020). Some minerals considered as characteristic of listvenitized ultramafic rocks still occur in the studied rocks (quartz, and minor magnesite veins) but isotopic analysis of magnesite from Szklary (Jedrysek, Halas 1990) points

to rather a supergene origin. Therefore, the contents of MgO and SiO_2 in Type I are not due to listvenitization but likely result from the presence of relicts of primary Mg-silicates and silica precipitation from fluid circulating within serpentinized peridotites.

In silicified serpentinites of Type II, the content of SiO_2 has been doubled in comparison to serpentinized peridotites. Such extremely high silica concentrations are close to those observed in many quartzites or quartz arenites (Frost, Frost 2014). Large enrichment in SiO_2 makes Type II overlap with silica listvenites (Boskabadi et al. 2020) (Fig. 8). However, silica listvenites could contain minor amounts of dolomite, sulfides and Cr-rich muscovite (Boskabadi et al. 2020; Gahlan et al. 2020), which are not observed in Type II. The studied samples chemically do not clearly overlap with birbirites, which have been previously described in Szklary Massif by Mikulski (2014) (Fig. 8). The main difference lies in the elevated content of MgO in silicified serpentinites of Type II, but this feature may be caused by the different methods used to determine whole-rock chemical composition. Relatively low LOI and magnesium content in Type II is consistent with microscopic observations and reflect minor amounts or even a complete lack of carbonates, as well as of various minerals with hydroxyl groups.

Most trace elements in partially serpentinized peridotites are characterized by concentrations below the detection limits (e.g., REEs). On the other hand, silicified serpentinites show higher REEs concentrations suggesting that trace elements were added at some stage of their development. Undoubtedly, the rare-earth elements could have been associated with Si-rich fluids (Salvi et al. 2000; Kempe et al. 2015). On the other hand, residual enrichment in REE by lateritization is also probable (Aiglsperger et al. 2016; Ulrich et al. 2019). Samples representing Type I and Type II show variable Ni and Co contents, which suggest that silicified serpentinites were affected by heterogeneous metals remobilization during intense chemical weathering of serpentinized peridotites and the supergene gain of silica within the lower part of saprolite horizon was strongly related to this process (Freyssinet et al. 2005; Ito et al. 2021).

6.3. Sources of silica for serpentinized peridotites

Silicified serpentinites can be interpreted as a product of at least two silicification processes, one related to the hydrothermal event and the second to supergene chemical weathering. The source of hydrothermal Si-rich fluid is currently unclear. The Szklary Massif is located within a shear zone, and hence new fluid conduits could have been produced during the deformation event. This scenario is probable because most of the silicification zones located in an abandoned quarry as well as single silica veins orientation correspond to the prevailing structural N-S trend of the Niemcza dislocation zone (Mazur, Puziewicz 1995). The higher K, Rb and Zr contents (Fig. 5-6) and occurrence of zircon inclusions in Type I silicified serpentinite may suggest that fluid influx was related to magmatism, which is well documented within the Niemcza zone. Carboniferous high K to shoshonitic monzodiorites crop out in the abandoned quarry, situated in Koźmice village, nearby the northern margin of the Szklary Massif (Pietranik et al. 2013). Zircons from these rocks yield magma emplacement ages 335.6 ± 2.3 Ma (Pietranik et al. 2013). Moreover, igneous dikes represented in particular by pegmatites, are located within the Szklary Massif itself. Monazite-(Ce) dated in LCT-type pegmatite yielded ages 383 ± 2 Ma, and therefore, the pegmatite-forming melt is concurrent with the anatectic melting in the Góry Sowie Massif (Pieczka et al. 2015). We suggest that the first stage of serpentinized peridotites silicification may be related to at least one of the aforementioned events, presumably accompanied by the presence of Si-rich fluid (Fig. 9a).

Subsequent silicification is caused by chemical weathering under tropical climate conditions, however the exact age of lateritic cover formation has not been established yet. According to Mikulski (2014) chemical weathering is contemporaneous with silicification and occurred at the turn of the Oligocene and Miocene. On the other hand, Dill (2017) considers the Late Cretaceous (Turonian – Campanian) as an actual age of weathering from the Szklary Massif, while in older studies the researchers suggest a Tertiary age (e.g., Niśkiewicz 1967; Dubińska 1995). Therefore, the second stage of serpentinites silicification occurred at least during the Late Cretaceous (Fig. 9b). Currently, both types of silica are visible in both types of silicified rocks but in different proportions. A possible scenario is that the most pronounced changes in the drainage conditions were at the contact of unweathered serpentinites with saprolite, which is why we observe the most advanced precipitation of silica during weathering at this contact. Original mesh texture of partially serpentinized peridotites and relics of primary minerals are visible in both types of silicified serpentinites, because they were formed from the same protolith. However, Type I display more frequent primary features of the protolith, owing to weaker weathering intensity. The silica of weathering origin coexists with older (hydrothermal) quartz generation, mostly in the rock/saprolite boundary. This suggests that certain fragments of partially serpentinized peridotites recorded both silicification stages (Fig. 9c).

7. Conclusions

Based on samples collected from newly described exposures of silicified serpentinites, located in the southern part of the Szklary Massif, we concluded that silicification is caused by at least two processes. The chemical and mineral composition, as well as the characteristic of quartz indicate that the earlier stage of silicification was related to the influx of epithermal Si-rich fluids. This fluid percolation led to the crystallization of hydrothermal quartz. We suggest that the presence of low-temperature mineralized fluids was caused by ca. 380 to 330 Ma magmatism which was widespread within this area. The following stage of ultramafic rocks silicification occurred not earlier than the Late Cretaceous, but likely before the Miocene. After the partial hydrothermal enrichment in silica, the same ultramafic rocks have been affected by the lateritic weathering process. Consequently, the majority of Mg-silicates were dissolved and magnesium was leached out. Thus, silicified serpentinites from the Szklary Massif have features characteristic for supergene as well as hydrothermal silicification.

Acknowledgments

This research belongs to one of the Priority Research Areas (POB) “Man, city, environment” implemented by the University of Wrocław as part of the Initiative of Excellence - Research University program (IDUB). The financial support for this work was provided by institutional funding of the Institute of Geological Sciences, the University of Wrocław by the Ministry of Science and Higher Education of Poland. We thank Alessia Borghini and Silvio Ferrero for their constructive comments, which significantly improved the final version of the text.

References

Aftabi, A., & Zarrinkoub, M., H. (2013). Petrogeochemistry of listvenite association in metaophiolites of Sahlabad region, eastern Iran: Implications for possible epigenetic Cu–Au ore exploration in metaophiolites. *Lithos, 156–159*, 186–203. DOI: 10.1016/j.lithos.2012.11.006.

Aiglsperger, T., Proenza, J. A., Lewis, J. F., Labrador, M., Svojtka, M., Rojas-Purón, A., Longo, F., & Ďurišová, J. (2016). Critical metals (REE, Sc, PGE) in Ni laterites from Cuba and the Dominican Republic. *Ore Geology Reviews*, *73*, 127–147. DOI: 10.1016/j.oregeorev.2015.10.010.

Aleksandrowski, P., & Mazur, S. (2002). Collage tectonics in the northeasternmost part of the Variscan Belt: the Sudetes, Bohemian Massif. *Geological Society, London, Special Publications, 201*(1), 237–277. DOI: 10.1144/GSL.SP.2002.201.01.12.

Auclair, M., Gauthier, M., Trottier, J., Jebrak, M., & Chartrand, F. (1993). Mineralogy, geochemistry, and paragenesis of the Eastern Metals serpentinite-associated Ni-Cu-Zn deposit, Quebec Appalachians. *Economic Geology*, *88*(1), 123–138. DOI: 10.2113/gsecongeo.88.1.123.

Awdankiewicz, M., Kryza, R., Turniak, K., Ovtcharova, M., & Schaltegger, U. (2021). The Central Sudetic Ophiolite (European Variscan Belt): Precise U-Pb zircon dating and geotectonic implications. *Geological Magazine*, *158*(3), 555–566. DOI: 10.1017/S0016756820000722.

Badura, J., & Dziemiańczuk, E. (1981). Szczegółowa mapa geologiczna sudetów 1:25 000, ark. Ząbkowice Śląskie. *Wydawnictwo Geologiczne*, Warszawa.

Boskabadi, A., Pitcairn, I. K., Leybourne, M. I., Teagle, D. A. H., Cooper, M. J., Hadizadeh, H., Nasiri Bezenjani, R., & Monazzami Bagherzadeh, R. (2020). Carbonation of ophiolitic ultramafic rocks: Listvenite formation in the Late Cretaceous ophiolites of eastern Iran. *Lithos*, *352–353,* 105307. DOI: 10.1016/j.lithos.2019.105307.

Butt, C. R. M., & Cluzel, D. (2013). Nickel laterite ore deposits: Weathered serpentinites. *Elements*, *9*(2), 123–128. DOI: 10.2113/gselements.9.2.123.

Čermáková, Z., Hradil, D., Bezdička, P., & Hradilová, J. (2017). New data on “kerolite–pimelite” series and the colouring agent of Szklary chrysoprase, Poland. *Physics and Chemistry of Minerals*, *44*(3), 193–202. DOI: 10.1007/s00269-016-0848-z.

Coleman, R. G. (1971). Petrologic and Geophysical Nature of Serpentinites. *GSA Bulletin*, *82*(4), 897–918. DOI: 10.1130/0016-7606(1971)82[897:PAGNOS]2.0.CO;2.

Dill, H. G. (2017). Residual clay deposits on basement rocks: The impact of climate and the geological setting on supergene argillitization in the Bohemian Massif (Central Europe) and across the globe. *Earth-Science Reviews*, *165*, 1–58. DOI: 10.1016/j.earscirev.2016.12.004.

Dong, G., Morrison, G., & Jaireth, S. (1995). Quartz textures in epithermal veins, Queensland - classification, origin, and implication. *Economic Geology*, *90*(6), 1841–1856. DOI: 10.2113/gsecongeo.90.6.1841.

Dubińska, E. (1995). Zróżnicowanie materiału wyjściowego zwietrzeliny a rozwój laterytowych rud niklu. *Przewodnik LXVI Zjazdu Polskiego Towarzystwa Geologicznego*, 207–212.

Dubińska, E., Bylina, P., Kozłowski, A., Dörr, W., Nejbert, K., Schastok, J., & Kulicki, C. (2004). U–Pb dating of serpentinization: hydrothermal zircon from a metasomatic rodingite shell (Sudetic ophiolite, SW Poland). *Chemical Geology*, *203*(3–4), 183–203. DOI: 10.1016/j.chemgeo.2003.10.005.

Dubińska, E., & Gunia, P. (1997). The Sudetic ophiolite: current view on its geodynamic model. *Geological Quarterly*, *41*, 1–20.

Dubińska, E., Sakharov, B. A., Kaproń, G., Bylina, P., & Kozubowski, J. A. (2000). Layer silicates from Szklary (Lower Silesia): from ocean floor metamorhism to continental chemical weathering. *Geologia Sudetica*, *33*(2), 85–105.

Duparc, L., Molly, E., & Borloz, A. (1927). Sur la Birbiriten une nouvelle roche. *Compte Rendu Des Séances de La Société de Physique et D’Histoire Naturelle de Genève*, *44*, 137–139.

Elias, M. (2002). Nickel laterite deposits – geological overview, resources and exploitation. *Centre for Ore Deposit Research, University of Tasmania, Hobart, Special Publication*, *4*, 205–220.

Flörke, O.W., Graetsch, H., Martin, B., Röller, K., Wirth, R. (1991). Nomenclature of micro-and non-crystalline silica minerals, based on structure and microstructure.

Neues Jahrbuch Mineralogie, *Abhandlungen*, *163*, 19–42.

Franke, W., & Żelaźniewicz, A. (2000). The eastern termination of the Variscides: terrane correlation and kinematic evolution. *Geological Society, London, Special Publications*, *179*(1), 63–86. DOI: 10.1144/GSL.SP.2000.179.01.06.

Frelinger, S. N., Ledvina, M. D., Kyle, J. R., & Zhao, D. (2015). Scanning electron microscopy cathodoluminescence of quartz: Principles, techniques and applications in ore geology. *Ore Geology Reviews*, *65*, 840–852. DOI: 10.1016/j.oregeorev.2014.10.008.

Freyssinet, PH., Butt, C. R. M., Morris, R. C., & Piantone, P. (2005). Ore-Forming Processes Related to Lateritic Weathering. In J. W. Hedenquist, J. F. H. Thompson, R. J. Goldfarb & J. P. Richards (Eds.), *One Hundredth Anniversary Volume* (pp. 681–722). Society of Economic Geologists. DOI: 10.5382/AV100.21.

Frost, B.R., & Frost, C.D. (2014). *Essentials of Igneous and Metamorphic Petrology.* Cambridge University Press. New York, USA.

Gahlan, H. A., Azer, M. K., Asimow, P. D., & Al-Kahtany, K. M. (2020). Petrogenesis of gold-bearing listvenites from the carbonatized mantle section of the Neoproterozoic Ess ophiolite, Western Arabian Shield, Saudi Arabia. *Lithos*, *372–373*, 105679. DOI: 10.1016/J.LITHOS.2020.105679.

Gibson, H. L., Watkinson, D. H., & Comba, C. D. A. (1983). Silicification; hydrothermal alteration in an Archean geothermal system within the Amulet Rhyolite Formation, Noranda, Quebec. *Economic Geology, 78*(5), 954–971. DOI: 10.2113/gsecongeo.78.5.954.

Golightly, J. P. (2010). Progress in Understanding the Evolution of Nickel Laterites. In R. J. Goldfarb, E. E. Marsh & T. Monecke (Eds.), *The Challenge of Finding New Mineral Resources, Global Metallogeny, Innovative Exploration, and New Discoveries* (pp. 451-485). Society of Economic Geologists. DOI: 10.5382/SP.15.2.

Götte, T., Pettke, T., Ramseyer, K., Koch-Muller, M., & Mullis, J. (2011). Cathodoluminescence properties and trace element signature of hydrothermal quartz: A fingerprint of growth dynamics. *American Mineralogist*, *96*(5–6), 802–813. DOI: 10.2138/am.2011.3639.

Götze, J. (2009). Chemistry, textures and physical properties of quartz — geological interpretation and technical application. *Mineralogical Magazine*, *73*(4), 645–671. DOI: 10.1180/minmag.2009.073.4.645.

Gunia, P. (2000). The petrology and geochemistry of mantle-derived basic and ultrabasic rocks from the Szklary Massif in the Fore-Sudetic Block (SW Poland). *Geologia Sudetica*, *33*(2), 71–83.

Gunia, P. (2007). Plagiogranites from the Szklary serpentinite massif, a component of the Sudetic ophiolite. *Granitoids in Poland, AM Monograph*, 1, 287–295.

Halls, C., & Zhao, R. (1995). Listvenite and related rocks: perspectives on terminology and mineralogy with reference to an occurrence at Cregganbaun, Co. Mayo, Republic of Ireland. *Mineralium Deposita*, *30*(3–4), 303–313. DOI: 10.1007/BF00196366.

Ito, A., Otake, T., Maulana, A., Sanematsu, K., Sufriadin, & Sato, T. (2021). Geochemical constraints on the mobilization of Ni and critical metals in laterite deposits, Sulawesi, Indonesia: A mass-balance approach. *Resource Geology*, *71*(3), 255–282. DOI: 10.1111/rge.12266.

Jedrysek, M. O., & Halas, S. (1990). The origin of magnesite deposits from the Polish Foresudetic Block ophiolites: preliminary $\delta^{13}C$ and $\delta^{18}O$ investigations. *Terra Nova*, *2*(2), 154–159. DOI: 10.1111/j.1365-3121.1990.tb00057.x.

Kempe, U., Möckel, R., Graupner, T., Kynicky, & Dombon, E. (2015). The genesis of Zr–Nb–REE mineralisation at Khalzan Buregte (Western Mongolia) reconsidered. *Ore Geology Reviews, 64*, 602–625. DOI: 10.1016/j.oregeorev.2014.05.003.

Klein, F., & Garrido, C. J. (2011). Thermodynamic constraints on mineral carbonation of serpentinized peridotite. *Lithos*, *126*(3–4), 147–160. DOI: 10.1016/j.lithos.2011.07.020.

Kryza, R., & Pin, C. (2010). The Central-Sudetic ophiolites (SW Poland): Petrogenetic issues, geochronology and palaeotectonic implications. *Gondwana Research, 17*(2–3), 292–305. DOI: 10.1016/j.gr.2009.11.001.

Lacinska, A. M., & Styles, M. T. (2013). Silicified serpentinite – A residuum of a Tertiary palaeo-weathering surface in the United Arab Emirates. *Geological Magazine, 150*(3), 385–395. DOI: 10.1017/S0016756812000325.

Mazur, S., Aleksandrowski, P., Kryza, R., & Oberc-Dziedzic, T. (2006). The Variscan Orogen in Poland. *Geological Quarterly*, *50*(1), 89 – 115.

Mazur, S., & Puziewicz, J. (1995). Mylonity strefy Niemczy. *Annales Societatis Geologorum Poloniae*, *64*, 23–52.

Mikulski, S. (2014). Silnie krzemionkowy zażelaziony metasomatyt (birbiryt) ze strefy zwietrzenia masywu serpentynitowego w złożu niklu w Szklarach na Dolnym Śląsku. *Biuletyn Państwowego Instytutu Geologicznego*, *458*, 61–72.

Moctar, D. O., Moukadiri, A., Boushaba, A., Lemine, S. O. M., & Dubois, M. (2019). Petrographical and Geochemical Characteristics of the Mauritanides Belts' Birbirites. In D. Doronozo, E. Schingaro, J. S. Armstrong-Altrin & B. Zoheir (Eds.), *Petrogenesis and Exploration of the Earth's Interior* (pp. 55–57). Springer Nature, Switzerland. DOI: 10.1007/978-3-030-01575-6_13.

Molly, E. W. (1959). Platinum deposits of Ethiopia. *Economic Geology*, *54*(3), 467–477. DOI: 10.2113/gsecongeo.54.3.467.

Niśkiewicz, J. (1967). Budowa geologiczna Masywu Szklar. *Rocznik Polskiego Towarzystwa Geologicznego*, *37*, 387–415.

Niśkiewicz, J. (2000). Pokrywa zwietrzelinowa masywu Szklar i jej niklonośność (The Szklary Massif nickel-bearing weathering cover). *Geologia Sudetica*, *33*(2), 107–130.

Pieczka, A., Cooper, M. A., & Hawthorne, F. C. (2019). Lepageite, $Mn_3^{2+}(Fe_7^{3+}Fe_4^{2+})\ O_3[Sb_5^{3+}As_8^{3+}O_{34}]$, a new arsenite-antimonite mineral from the Szklary pegmatite, Lower Silesia, Poland. *American Mineralogist*, *104*(7), 1043–1050. DOI: 10.2138/am-2019-6903.

Pieczka, A., Szuszkiewicz, A., Szełęg, E., Janeczek, J., & Nejbert, K. (2015). Granitic pegmatites of the Polish part of the Sudetes (NE Bohemian massif, SW Poland). *7th International Symposium on Granitic Pegmatites, Fieldtrip Guidebook* (pp. 73–103).

Pietranik, A., Storey, C., & Kierczak, J. (2013). The Niemcza diorites and monzodiorites (Sudetes, SW Poland): A record of changing geotectonic setting at ca. 340 Ma.

Geological Quarterly, *57*(2), 325–334. DOI: 10.7306/gq.1084.

Rusk, B. (2012). Cathodoluminescent Textures and Trace Elements in Hydrothermal Quartz. In J. Götze & R. Möckel (Eds.), *Quartz: Deposits, Mineralogy and Analytics* (pp. 307–329). Springer. DOI: 10.1007/978-3-642-22161-3_14.

Salvi, S., Fontan, F., Monchoux, P, Williams-Jones, A. E., & Moine, B. (2000). Mobilization of High Field Strength Elements in Alkaline Igneous Systems: Evidence from the Tamazeght Complex (Morocco). *Economic Geology, 95*(3), 559–576. DOI: 10.2113/gsecongeo.95.3.559.

Schaltegger, U. (2007). Hydrothermal Zircon. *Elements*, *3*(1), 51–79. DOI: 10.2113/gselements.3.1.51.

Sherman, G. D., Kanehiro, Y., & Matsu Saka, Y. (1953). Role of dehydration in development of the laterite crust. *Pacific Science, 7*, 438–446.

Spiridonov, E. M. (1991). Listvenites and zodites. *International Geology Review*, *33*(4), 397–407. DOI: 10.1080/00206819109465698.

Ulrich, M., Cathelineau, M., Muñoz, M., Boiron, M.-C., Teitler, Y., & Karpoff, A. M. (2019). The relative distribution of critical (Sc, REE) and transition metals (Ni, Co, Cr, Mn, V) in some Ni-laterite deposits of New Caledonia. *Journal of Geochemical Exploration*, *197*, 93–113. DOI: 10.1016/j.gexplo.2018.11.017.

Wiewióra, A. & Szpila, K. (1975). Nickel Containing Regularly Interstratified Chlorite-Saponite from Szklary, Lower Silesia, Poland. *Clays and Clay Minerals*, *23*, 91–96. DOI: 10.1346/CCMN.1975.0230202

Received: 25 January 2022
Accepted: 17 May 2022
Handling Editor: Silvio Ferrero